Scientia Iranica D (2023) 30(4), 1330–1341

SCIENTIA IRANICA

Sharif University of Technology
Scientia Iranica
Transactions D: Computer Science & Engineering and Electrical Engineering
http://scientiairanica.sharif.edu

Design, optimization, and control of a linear tubular machine integrated with levitation and guidance for maglev applications

H.R. Esfahanian[a], S. Hasanzadeh[a,*], M. Heydari[a], and J.M. Guerrero[b]

a. *Departmanet of Electerical and Computer Engineering, Qom University of Technology, Qom, Iran.*
b. *Department of Energy Technology, Aalborg University, Aalborg, Denmark.*

Received 9 January 2021; received in revised form 24 August 2021; accepted 18 October 2021

KEYWORDS
Magnetic levitation (maglev) trains;
Linear Induction motor (LIM);
Finite Element Method (FEM);
Optimization;
Integrated controller.

Abstract. Nowadays, with the growing population, demand for efficient public transportation systems has increased. Magnetic levitation (maglev) trains are one of the best choices for the future. There are three separate systems in a classical magnetic train to achieve desirable performance. Hence, several control systems and sensors are essential for train operation. Accordingly, the classical maglev trains include complex structures and they are so expensive. This paper presents the design, optimization, and control of a combined magnetic train structure with the integrated performance of suspension and guidance and a complementary propulsion system. These combined topologies provide a simple design, enure a more convenient movement, and reduce construction and operation costs.

1. Introduction

Nowadays, with the increase of population, demand for new public transportation systems has increased. These systems must be rapid and secure. Among the available options, the magnetic levitation (maglev) train is one of the best choices that has many advantages over the classical trains: (1) the fastest ground transportation system; (2) lower power consumption; (3) less noise and vibration; (4) higher level of safety and convenience; (5) better performance of acceleration and deceleration and also, better movement on a slope; (6) reduction in maintenance costs; (7) elimination of gear, coupling, axles, and bearings; (8) less impressionability to weather conditions; and 9) environmentally friendliness. So far, much research has been done on these train-based technologies, such as modeling and analyzing linear electric machines, superconducting magnets, and permanent magnets [1–3]. Three forces are required to achieve the desired performance in the case of a maglev train: (1) levitation force that lifts the train; (2) guidance force that prevents train derailing; (3) propulsion force generated by a linear motor to move the train. There are three separate systems in the conventional maglev trains to generate these three forces [1,4–6]. Thus, many sensors and control systems are necessary for the operation of the train that makes classical maglev trains complex and expensive. Furthermore, control of the levitation force is a severe challenge for engineers. In addition, it is one of the most challenging operations to apply in classical maglev trains [4,7]. Some combined topologies are developed to eliminate these challenges that provide more convenient movement, simpler structure, and cheaper operation [4,8–10]. Among suspension technologies used in maglev trains, the suspension system is inherently unstable in

*. *Corresponding author.*
E-mail addresses: Esfahanian.h@qut.ac.ir (H.R. Esfahanian); hasanzadeh@qut.ac.ir (S. Hasanzadeh); heydari@qut.ac.ir (M. Heydari); joz@energy.aau.dk (J.M. Guerrero)

doi: 10.24200/sci.2021.57416.5231

Electromagnetic Suspension (EMS) technology due to the nonlinear dynamic model. Therefore, the control of levitation force is necessary for this technology [1,11]. So far, different control techniques have been used to control the levitation force of the maglev trains. In most articles related to the suspension of magnetic trains, only the presentation and analysis of a control technique and improvement of the control process are considered. Indeed, usual suspension structures are used for mathematical modeling and control, while the design and geometry of the suspension structure are not considered. Another problem of classical magnetic trains, which use separate systems for suspension and guidance, is the electromagnetic coupling effect of the levitation and guidance systems (of these two separate systems), leading to the controlled disturbance in both systems and the complexity of the control process [11–13].

This paper presents a new magnetic train topology with integrated suspension and guidance and a complementary propulsion system. The proposed hybrid structure utilizes two separate force generation systems: a system for simultaneously achieving suspension and guidance performance and another system for propulsive force generation. In addition, the propulsion system serves as a complement for the suspension and guidance performance and supports the first system. The propulsion system has a complementary role and supports the first system in terms of suspension and guidance performance. Next, we will introduce each of these designed systems and then, provide a suitable controller for the integrated suspension and guidance system. Next, we will evaluate this controller.

2. The combined topology of the magnetic train

The combined structure of the magnetic train is shown in Figure 1. The electromagnets are embedded at a 45-degree angle to the horizontal surface on the arms on two sides of the wagon for suspension and guidance performance. The propulsion force of the train is supplied through several linear tubular induction motors located below the train at the center of the rail or path (energization on the vehicle onboard). It should be noted that these linear motors have a common secondary part.

2.1. Integrated suspension and guidance system

In classical magnetic trains, given that suspension electromagnets are at an angle of zero degree to the horizontal surface, the gap distance and its changes, as well as the balance between the magnetic force of the electromagnets and the weight of the train, are measured perpendicular to the horizontal surface. The suspension operation leads to maintaining the vertical gap distance at the optimum level and preventing any vertical displacement due to disturbances that affect suspension system in vertical alignment. Similarly, guidance operation in classical magnetic trains prevents lateral deviations (deviations to the right or left) under the effect of lateral disturbances. Thus, in general, it can be concluded that the suspension system and the guidance system in a classical magnetic train prevent train movement in vertical and horizontal directions.

In the proposed hybrid structure featuring a new geometry of the position of suspension electromagnets relative to the classical maglev structures, the electromagnetic attraction forces created by them, in addition to the suspension performance, will act as guidance forces. In doing so, we no longer need a separate magnetic system to generate guidance force, and this will simplify and cheapen the maglev structure and reduce the need for control systems and sensors.

Figure 2 shows the vector diagram of forces in the proposed suspension system. According to the 45-degree angle of electromagnets to the horizontal surface, by parsing the weight force into two com-

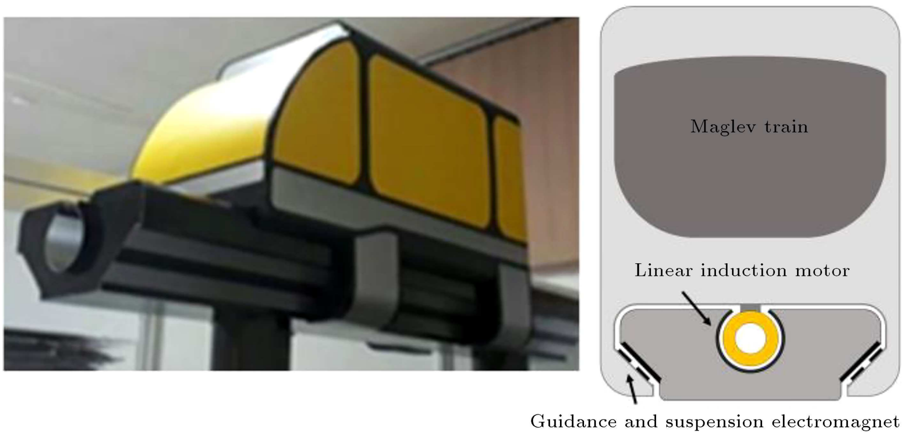

Figure 1. The combined structure of the magnetic train.

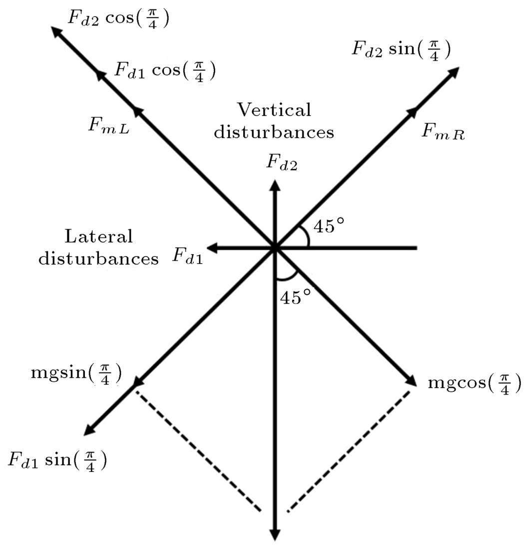

Figure 2. Vector diagram of forces in the integrated suspension and guidance system.

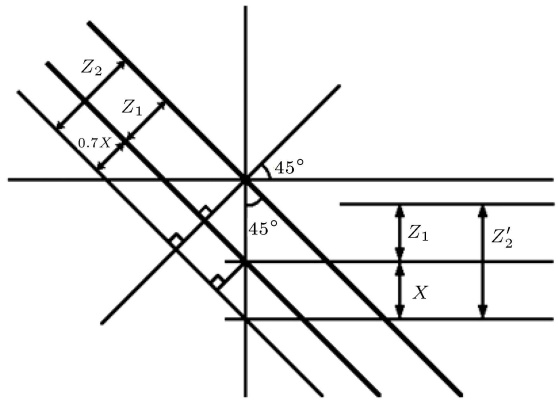

Figure 3. Comparison of air gap deviation in the proposed suspension system with the classic suspension system.

ponents along the magnetic forces produced by two electromagnets and in opposite directions, to achieve balance, the magnetic force of each electromagnet must be equal to the weight component force in its direction. Any disturbances of force along with the vertical and horizontal directions (irrespective of their direction), similar to the weight force, can be separated into two components along with two electromagnet forces. Therefore, despite disturbances, the control system changes two electromagnet forces to balance the forces in the direction of each electromagnet and maintains both air gaps in their desired amount. Therefore, what is described as the integrated performance of suspension and guidance in the proposed system is achieved by controlling the air gap. In other words, any horizontal and vertical displacement will change the desired amount of air gap.

In addition to the suspension and guidance along with simultaneously maintaining the air gap in the integrated suspension and guidance system, another issue that should be considered as an advantage of the proposed structure over the suspension system of classical magnetic trains is the reduced impact of air gap from vertical deviations and lateral deviations. According to Figure 3, if Z_1 is considered ideal air gap in the suspension system of a classic magnetic train, as well as in the integrated suspension and guidance system, and if vertical deviations X affect both systems, the new air gap in the suspension system of the classical magnetic train (Z_2') and the air gap in the integrated suspension and guidance system (Z_2) are obtained by Eqs. (1) and (2), respectively:

$$Z_2' = Z_1 \pm X, \tag{1}$$

$$Z_2 = Z_1 \pm 0.7X. \tag{2}$$

Based on the comparison of the two relations, a 30% reduction of air gap changes due to the effect of vertical deviations is determined in the proposed system with respect to the suspension system of classical magnetic trains. Similarly, concerning the integrated suspension and guidance performance, there will be a 30% reduction of air gap changes due to the impact of lateral deviations with respect to the classical magnetic train guidance system.

Figure 4 shows the problem of (Electromagnetic coupling effect) magnetic interference of the suspension system and the guidance system in the classical magnetic trains. However, the problem will be resolved in the proposed hybrid structure due to the integrated suspension and guidance by one system.

2.2. Complementary propulsion system

As mentioned earlier in the beginning of this section, linear air-cored tubular induction motors are used to generate propulsion force in the proposed structure in this paper. This type of linear induction motor, like a rotary induction motor, consists of two main parts: (1) primary or drive coils that are installed underneath of the wagons and (2) the secondary part that consists of an aluminum slit sleeve that surrounds the drive coils and is located on the rail. The tubular linear induction motor operates similarly to classical three-phase induction motors. A traveling magnetic wave is created by the three-phase excitation in the drive coils that induce currents in the sleeve. Both drive coils and sleeve currents generate the resultant magnetic flux. The flux density can be decomposed into two components: one in the longitudinal direction and the other in the radial direction. Interaction between the radial component of the flux density and the sleeve current generates the propulsion force.

In contrast, the flux density component in the longitudinal direction interacts with the sleeve current to produce the radial forces [4,14]. The theory of the production of these forces was presented in [14]. Linear

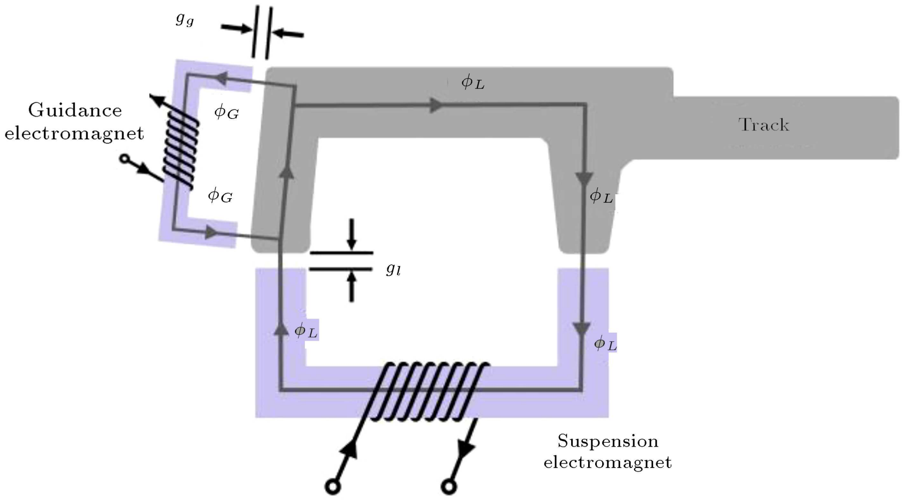

Figure 4. Electromagnetic coupling effect of the suspension system and the guidance system in the classical magnetic train.

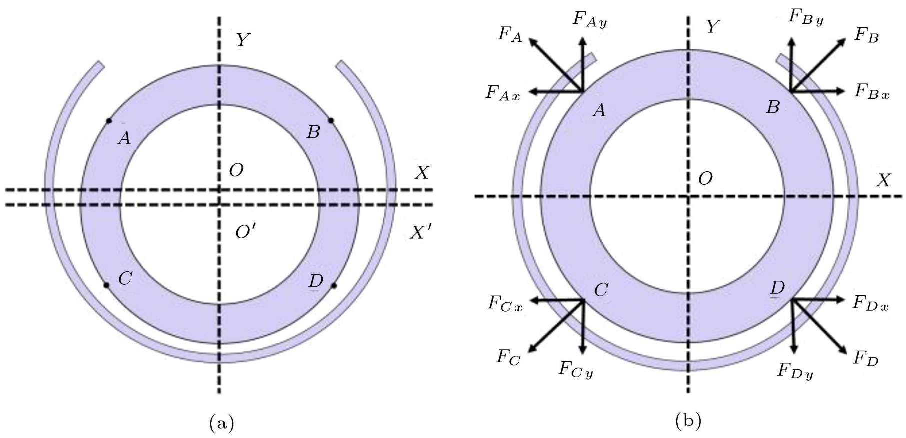

Figure 5. (a) Motor cross-section in a balanced position, (b) The movement of the drive coils in the direction of the y axis.

Induction Launchers (LIL) are another application of linear air-cored tubular induction motors such that studying them gives a better view of these types of motors [15].

Since the drive coils are supported only by electromagnetic force rather than physical connection with the secondary part, the center (axis) of the drive coils may not coincide with that of the sleeve for many reasons namely vibration, disturbances, gravity, or other causes. When the drive coils are placed in the secondary center, the radial forces around them are balanced. However, if the central axes of the drive coils and sleeve do not coincide, the radial forces around the drive coils are not balanced and there exists a transverse force due to the asymmetry. This force is called the restoring force, and it is the fundamental tool for the analysis of the dynamic motion of the coil drives in the transverse (radial) direction [16]. A 3D Finite Element Method (FEM) analysis presented in [4] shows that the restoring force acting on the moving part is satisfactory to levitate and guide the moving part and deal with the low-damping problem, which is one of the most important dynamic stability problems that occurs in the maglev systems.

In the maglev system, as mentioned earlier, the opening of the sleeve causes the radial forces to be unbalanced and generates the restoring force that rebalances the radial forces. It can be seen from Figure 5(a) that x components of the radial forces at points A and B and also, at points C and D (x-axis and y-axis are considered as the symmetrical axes) are the same in magnitude, but opposite in direction. There is the same balance between the y components of the radial forces at not only points A and C but also points B and D. This balance of the drive coils is achieved by the restoring force that eliminates the effect of the opening angle of the sleeve. Any change from the balanced position of the drive coils, shown in Figure 5(a), makes the radial forces unbalanced. Figure 5(b) shows the movement of the drive coils in the direction of the y-axis. This will cause the y components of the radial forces at points A and C and also, points B and D to be unequal [16]; however, due to the restoring force that exists between two noncoaxial circular coils, the moving part is placed at the center again [15]. In order to calculate the equivalent force between sleeve and drive coils, instead of integrating the force on the differential element over the entire loop of the drive coils, it is better to distinguish the two force elements in each half of the drive coil circle. As a result, these two forces are in the direction opposite to each other and the difference between them is defined as the restoring force:

$$F_s = F_1 - F_2, \tag{3}$$

where F_1 and F_2 are the force elements in the left and right half loops of the drive coils, respectively, and F_s is the restoring force. F_1 and F_2 forces are obtained by integrating the force on the differential element over the left and right half loops of the drive coils, respectively [15]. The two forces, F_1 and F_2, are equal in a balanced condition and the restoring force will be zero [16].

Due to the performance of the motor and the nature of the restoring force, the complementary role of the motor for the integrated suspension and guidance system is determined. As stated, the performance of the integrated suspension and guidance system in the proposed structure is such that it avoids any horizontal and vertical deviations of the wagon while maintaining the desired air gap. According to Figure 1, in the desired air gap of the integrated suspension and guidance system, the designed structure resembles the motor in the balance condition (central axes of the drive coils and sleeve coincide). Therefore, any horizontal and vertical deviation of the wagon, which causes the change of the air gap and motor unbalancing, will be simultaneously eliminated by both systems. The benefit of using this type of motor in the proposed structure is that the suspension performance and guidance produced by the motor, in contrast to the integrated suspension and guidance system, is achieved without the need for a control system. In other words, the inherent self-levitating and self-guiding properties are provided only by the restoring force between two main parts of the motor [4].

After expressing the performance of the propulsion system and its inherent guidance and suspension, extracting and analyzing the components of the motor force and improving them represent an introduction to designing the controller of the integrated suspension and guidance system at the end of this paper. Because any disturbance in the performance of the motor disturbs the control process of the air gap, in other words, if the proposed structure is in a balanced condition, there should not be any force of the motor on the suspension and guidance electromagnets. In the following, by performing a 3D modeling of FEM in Maxwell software, the components of the motor force are extracted and the process of improving its performance will be presented.

3. 3D modeling and optimization of propulsion system using FEM

3D modeling of the motor is presented considering the design conditions, the basic design criteria given in [4,17], and its dimensions. According to Figure 6, motor modeling is done such that the opening angle of the sleeve is placed between the x and y axes. In other words, the x-axis and y-axis and the motor cross-section are symmetrical to the vertical axis. Since the moving part is placed in the center and due to the symmetry of two axes, x and y, the magnitude of the radial forces in the x-axis must be equal to the magnitude of the radial force in the y-axis. The 3D modeling of the motor in Maxwell software is shown in Figure 7.

The analysis begins to access the forces acting on the moving part on the x, y, and z axes. Figure 8 shows the forces. Although the motor dimension was obtained by using design conditions and basic design criteria in [4,17], as shown in Figure 8, the radial forces had minor differences; thus, eliminating or reducing the difference between them leads to a more desirable performance. This paper uses an alternative method to achieve optimal performance utilizing 3D FEM analysis. Therefore, by using a parametric simulation, only the radius of the sleeve is changed with the specified steps (0.5 mm) around the nominal value (32 mm). Increase in the secondary radius leads to the reduction of the force components.

In the following, their RMS (Root Mean Square) values in a steady state are utilized to compare waveforms. As shown in Figure 9, to determine the effect of changing the radius of the sleeve on force components, the RMS values of each force must be obtained as a

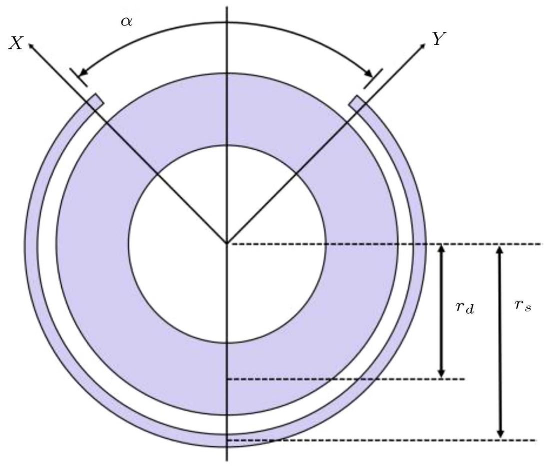

Figure 6. The cross-section of the simulation model.

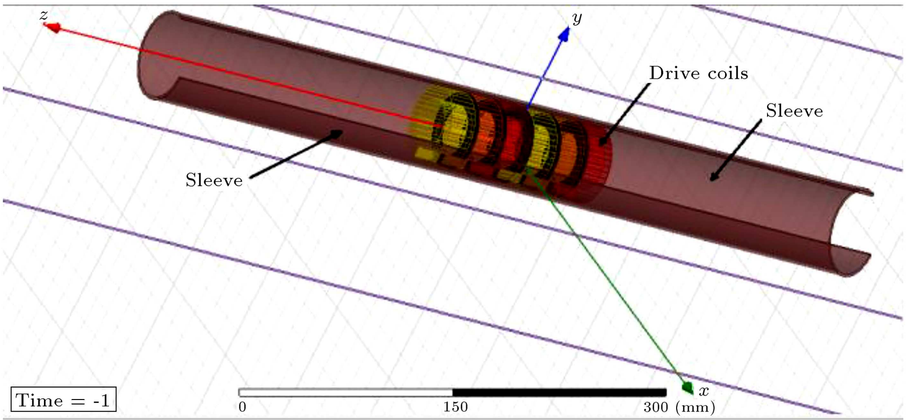

Figure 7. 3-D simulation modeling of the motor in Maxwell software.

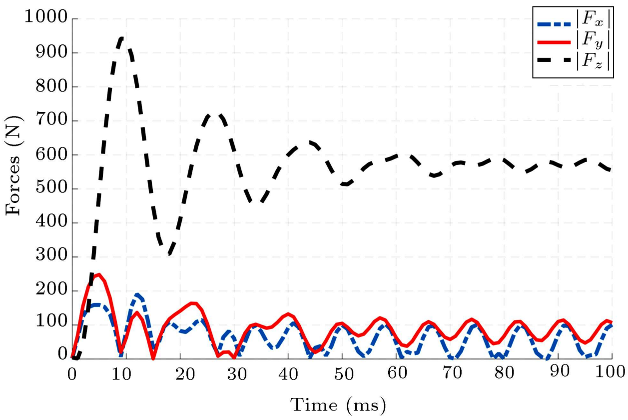

Figure 8. Forces acting on the moving part of the motor.

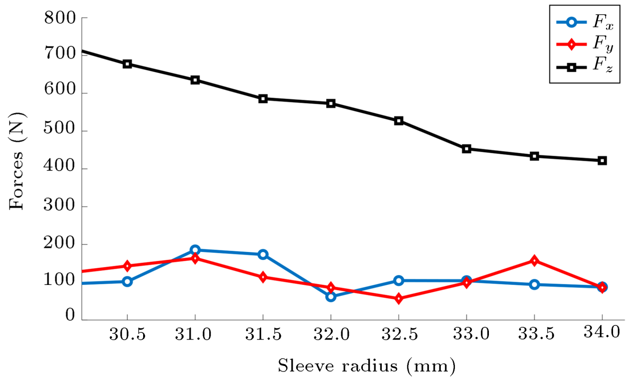

Figure 9. Changes in force components with the change of secondary radius.

function of radius. As shown in Figure 9, the RMS values of the forces decrease upon increasing the air gap or increasing the radius of the sleeve. Therefore, a range that contains a value less than the initial radius of the sleeve will be desirable by performing another parametric simulation with a minor step (0.05 mm) in the range of 30 to 32 mm for sleeve radius. According to the results shown in Figure 10 and Table 1, at a radius of 30.7 mm, the radial forces have the least difference.

Based on the results shown in Figure 11, by

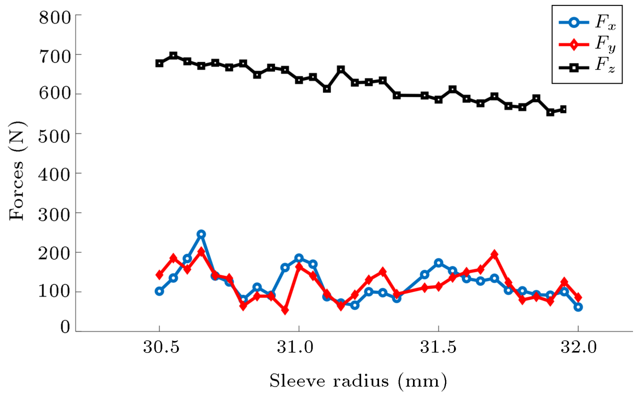

Figure 10. Changes in force components with the change of secondary radius.

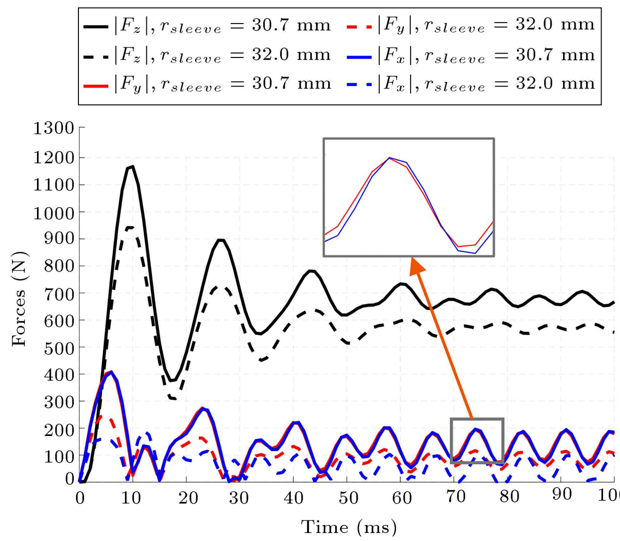

Figure 11. Comparison between force components before and after optimization.

replacing the optimal radius obtained from parametric simulations (30.7 mm) with the initial value, the difference between radial forces is reduced by 96%. In addition, the amplitude of the force components increases, which is highly desirable.

Table 1. Results of parametric simulation.

Sleeve radius (mm)	RMS (coil force. force_x) (N)	RMS (coil force. force_y) (N)
30.5	101.7484164	142.986268
30.55	135.1463087	185.3646056
30.6	184.3090923	156.802813
30.65	245.7121226	201.8437067
30.7	**140.1078119**	**141.6969531**
30.75	125.0982781	134.4862308
30.8	80.74267072	64.42590301
30.85	111.9342799	89.26949629
30.9	91.34702088	89.19752575
30.95	161.5155959	54.2226583
31	185.3727095	163.3875246
31.05	170.0994439	140.5974931
31.1	87.77955837	95.10431383
31.15	71.90093814	64.02198813
31.2	66.29826361	92.67014693
31.25	100.4469585	130.5362383
31.3	98.05764367	150.9641208
31.35	83.63232552	94.43662876
31.45	143.7374532	110.4886499
31.5	173.4268767	113.6014034
31.55	153.3003984	136.4016887
31.6	133.6854658	149.8584951
31.65	127.3928041	156.3621002
31.7	134.446692	194.8343938
31.75	104.1294056	123.6723358
31.8	102.69293	79.81950474
31.85	92.93456248	87.53540343
31.9	91.7297089	76.18283235
31.95	100.58268	125.2534449
32	61.7409704	85.86895861

4. Control of integrated suspension and guidance system

4.1. Modeling of suspension and guidance electromagnets

In order to design a control system, the mathematical modeling of the integrated suspension and guidance system consists of three categories of relationships: (1) the relationships of the magnetic circuit of the electromagnets; (2) the electrical circuit relationships of the electromagnets; and (3) the dynamic relations associated to the application of the magnetic force of the electromagnets to the integrated suspension and guidance system. Therefore, if the electromagnets placed on two arms in front of each other (Figure 1) are considered as a unit of suspension and guidance, the two systems of Eqs. (4) and (5) describe the relations of each electromagnet in a unit of suspension and guidance:

$$F_{mf_1} = \frac{\mu_0 AN^2}{4}\left(\frac{I_1}{Z_1}\right)^2,$$

$$V_1 = rI_1 + \frac{N^2\mu_0 A}{2Z_1}\dot{I}_1 - I_1\frac{N^2\mu_0 A}{2Z_1^2}\dot{Z}_1,$$

$$F_{mf_1} - \frac{\sqrt{2}}{2}mg = m\ddot{Z}_1, \tag{4}$$

$$F_{mf_2} = \frac{\mu_0 AN^2}{4}\left(\frac{I_2}{Z_2}\right)^2,$$

$$V_2 = rI_2 + \frac{N^2\mu_0 A}{2Z_2}\dot{I}_2 - I_2\frac{N^2\mu_0 A}{2Z_2^2}\dot{Z}_2,$$

$$F_{mf_2} - \frac{\sqrt{2}}{2}mg = m\ddot{Z}_2. \tag{5}$$

In each of the two systems of Eqs. (4) and (5), the first formula corresponds to the electromagnetic circuit of the electromagnet, while the second is associated with the electrical circuit of the electromagnet, and the third describes the dynamic of the electromagnet in the unit of suspension and guidance. The parameters used in two systems of Eqs. (4) and (5) are given in Table 2.

Since the purpose of controlling the integrated suspension and guidance system is to achieve the desired air gap by controlling the voltage applied to the electromagnets, the nonlinearity of the system dynamics is evident. In fact, the magnetic force of the electromagnets is proportional to the inverse square of the air gap $\left(F_{mf} \sim \frac{1}{Z^2}\right)$.

4.2. State-space mode of the Integrated Suspension and Guidance system

Given the relations expressed in the system of Eqs. (4) and (5), the air gap, the first derivative of the air gap, and the current are determined as the state variables describing the behavior of a unit of suspension and guidance; therefore, the state vector of the system is in accordance with Eq. (6):

$$X = \begin{bmatrix} x_1 & x_2 & x_3 & x_4 & x_5 & x_6 \end{bmatrix}^T$$
$$= \begin{bmatrix} Z_1 & \dot{Z}_1 & Z_2 & \dot{Z}_2 & I_1 & I_2 \end{bmatrix}^T. \tag{6}$$

By replacing the state vector variables in two systems of Eqs. (4) and (5), the representation of the nonlinear

Table 2. Parameters used in two systems of Relations (4) and (5).

Symbol	Quantity	Measurement unit
I_1 and I_2	Dc currents of electromagnets	A = Ampere
r	Coil's resistance of electromagnets	Ω = Ohm
Z_1 and Z_2	Air gaps of electromagnets	m = Metre
m	The mass applied to the suspension unit	kg = Kilogram
g	Gravitational acceleration	(m/s) ^{2} = Meter/second^2
F_{mf1} and F_{mf2}	Magnetic force of electromagnets	1 G $\rightarrow 10^3/(4\pi)$ A/m
μ_0	Vacuum permeability	H/m = Henry/metre
A	Cross section of electromagnets	m^2 = metre^2
N	Number of turns of electromagnet's coil	–
v_1 and v_2	Electromagnet's voltage	V = Volt

state space of a suspension and guidance unit is obtained in Eq. (7), where $\rho = \mu_0 A N^2$:

$$\begin{aligned}\dot{x} &= f(x,u)\\ &= \begin{bmatrix} \dot{x}_1 & \dot{x}_2 & \dot{x}_3 & \dot{x}_4 & \dot{x}_5 & \dot{x}_6 \end{bmatrix}^T\\ &= \begin{bmatrix} f_1 & f_2 & f_3 & f_4 & f_5 & f_6 \end{bmatrix}^T\\ &\begin{bmatrix} x_2 \\ \frac{-\rho}{4m}\left(\frac{x_5}{x_1}\right)^2 + \frac{\sqrt{2}}{2}g \\ x_4 \\ \frac{-\rho}{4m}\left(\frac{x_6}{x_3}\right)^2 + \frac{\sqrt{2}}{2}g \\ \frac{-2r}{\rho}x_1x_5 + \frac{x_2x_5}{x_1} + \frac{2x_1u_1}{\rho} \\ \frac{-2r}{\rho}x_3x_6 + \frac{x_4x_6}{x_3} + \frac{2x_3u_2}{\rho} \end{bmatrix}.\end{aligned} \tag{7}$$

4.3. Designing the optimized controller for the integrated suspension and guidance system

Despite the nonlinear model of the proposed approach and also, the advantages and widespread use of linear control systems in controlling the nonlinear systems, after linearization in this section, the nonlinear model of the integrated suspension and guidance unit namely an optimal linear control technique called Linear Quadratic Regulator (LQR) will be used for control [17]. Since the system has no equilibrium point, a new system with an origin equilibrium point is obtained by applying the changes in variables according to Eqs. (8) and (9) after determining a specific point as an operation point or nominal point of the system (x_r, u_r). Therefore, it is possible to design an LQR controller for a new system after linearizing it around the origin.

$$\bar{x} = x - x_r, \tag{8}$$

$$\bar{u} = u - u_r. \tag{9}$$

Regarding the changes in the variables expressed in Eqs. (8) and (9), if the variables or inputs in the new system move to the origin $((\bar{x}=0), (\bar{u}=0))$, the states in the initial system will move to the specified operation point $((x = x_r), (u = u_r))$.

In order to determine the operating point or nominal point, by setting the first and third variables of the state vector (air gaps) and assuming no changes in the operation point, other states, as well as the corresponding inputs with the nominal point, are obtained by using Eq. (6) and through Eqs. (9) and (10):

$$x_r=\left[x_{1r}\ \ 0\ \ x_{3r}\ \ \ 0\ \ \sqrt{\tfrac{2\sqrt{2}mg}{\rho}}x_{1r}\ \sqrt{\tfrac{2\sqrt{2}mg}{\rho}}x_{3r}\right]^T, \quad (10)$$

$$u_r=\left[\ u_{1r}\quad u_{2r}\ \right]^T=\left[\ rx_{5r}\quad rx_{6r}\ \right]^T. \quad (11)$$

After determining the nominal point, by applying the changes in the variables in Eqs. (8) and (9) to the nonlinear state space of the system in Eq. (7) and the linearization of the new system around the origin, the state matrix of the linear system is obtained by Eq. (12) as shown in Box I. As can be seen in the matrix Eq. (12), due to the zero values of the mutual entries of the first and third, second and fourth, and fifth and sixth, the states of each of the two electromagnets in a unit of suspension and guidance are independent of other. Therefore, by transforming the state vector to a triple vector in accordance with Eq. (13), the design of the control system can be done for an electromagnet:

$$x=\left[\ Z_1\quad \dot{Z}_1\quad I_1\ \right]^T. \quad (13)$$

The optimal control of LQR is expressed for a linear system in Eq. (14). In fact, in this control technique, which is a subset of the family of state feedback controllers, inputs to the system are constructed according to a combination of state variables [18].

$$u=-kx. \quad (14)$$

The feedback gain matrix in Eq. (14) (K) is calculated to minimize the cost function of Eq. (15). By minimizing the cost function, which means minimizing specific errors in the control process, the poles of the closed-loop system are located in places called optimal locations of the poles [18].

$$J=\int_0^{\infty}\left(x^TQx+u^TRu+2x^TNu\right)dt. \quad (15)$$

The matrices N, R, Q in Eq. (14) include the controlling (weighted parameters) parameters of the state error, the importance of the inputs, and the importance of multiplication of state error in the control inputs, respectively, set by the designer. The feedback gain matrix K is calculated via Eq. (16) [18]:

$$K=R^{-1}\left(B^TP+N^T\right), \quad (16)$$

where P is obtained from the solution of the continuous Roquette algebraic Eq. (17) [18]:

$$A^TP+PA-(BP+N)\,R^{-1}\left(B^TP+N^T\right)+Q=0. \quad (17)$$

To design an optimal LQR controller for an electromagnet in a unit of suspension and guidance, according to the three entries of the state vector expressed in Eq. (13), the weighted matrix Q is a 3×3 matrix, which is initially considered as a unit diagonal matrix. In addition, given that the system has one input (the voltage applied to the electromagnet's coil), the value of the weighted matrix R is equal to one. Assuming that the state error and input of the system do not interact with each other, the matrix N is considered zero. After determining the weighted matrices and designing the optimal LQR controller, the optimal feedback gain matrix is obtained using Eq. (18):

$$K=[-8713.3\quad -136.21\quad 5.9314]. \quad (18)$$

As shown in Figure 12, by applying the designed linear controller to the nonlinear system of an electromagnet, the result of controlling the air gap in the presence of disturbances and changing the nominal point is obtained, as shown in Figure 13.

Given that the weighted matrices are designed by the designer for achieving an optimal function in the control response, in the following, the entries of the matrix Q are changed so that a better control response can be achieved. It was found that upon changing (increasing) the entries of the matrix Q, the third entry of the matrix corresponding to the electromagnet current error would have a significant effect on the control response, while the impact of the change in the entries corresponding to the first and second state errors on the frequency response form can

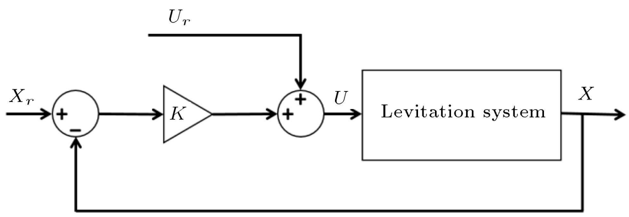

Figure 12. Controlling the nonlinear system of an electromagnet.

$$\begin{bmatrix} 0 & 1 & 0 & 0 & 0 & 0 \\ 1386.9 & 0 & 0 & 0 & -1.3284 & 0 \\ 0 & 0 & 0 & 1 & 0 & 0 \\ 0 & 0 & 1386.9 & 0 & 0 & -1.3284 \\ 0 & 1044.1 & 0 & 0 & -7.8595 & 0 \\ 0 & 0 & 0 & 1044.1 & 0 & -7.8595 \end{bmatrix}. \quad (12)$$

Box I

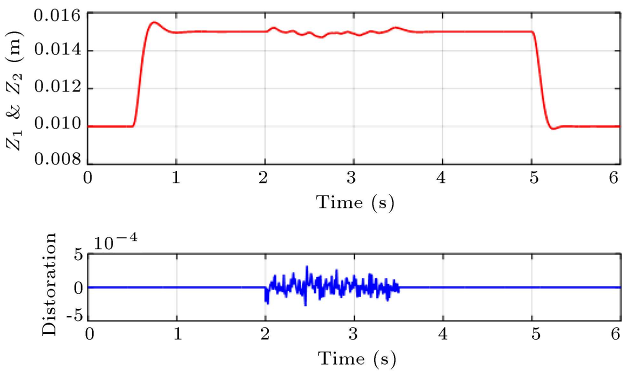

Figure 13. Controlling the air gap in the presence of disturbance and with changing the nominal point.

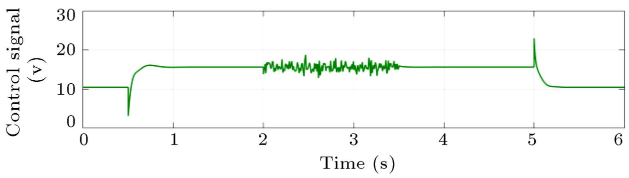

Figure 14. Control signal in the case that Q be a unit diagonal matrix.

be ignored. The amount of the current justifies this finding, compared to the air gap at the nominal point ($I \cong 100$ z). Another point that needs to be considered in finding a better control response is the practical limitations of the control signal. Figure 14 shows the control signal in the case that Q is a unit diagonal matrix. According to Figure 15, the control signal is associated with a mutation when the operation point is changed ($T = 0.5$ s and $T = 5$ s). In practice, the values of these mutations cannot be considered more than four times the signals' initial values since it is impossible to construct them by operators. Therefore, by considering the effect of the weighted matrix Q entries on the control response in this system and a triple allowable range of control signal mutations compared to the initial values, the first and second entries of Q are assumed constant. The third entry increases until the control signal does not exceed the specified range. After several simulations, it was determined that by replacing the number 33 with the third entry value of the matrix Q, the control signal mutation remained in the specified range, the speed of the control response increased (reduction of the rise time), and its overshoot decreased. The position of the control signal mutation in the range of three times the initial value and the improvement of the control response by changing entries of the matrix Q are shown in Figures 15 and 16, respectively.

5. Conclusion

This paper first introduced a magnetic train topology

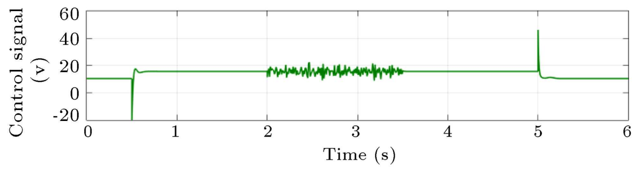

Figure 15. Position of the control signal mutation in the range of three times the initial value.

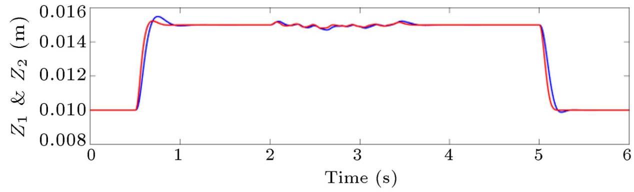

Figure 16. Improvement of the control response by changing entries of the matrix Q.

with integrated suspension and guidance and a complementary propulsion system. Subsequently, using 3D modeling of finite element method, the components of propulsion system force were extracted, analyzed, and optimized. After optimizing the performance of the propulsion system and reducing its impact on the integrated suspension and guidance system, the nonlinear state space of a unit of integrated suspension and guidance system was obtained with mathematical modeling. Then, by determining the operation point, changing the variables, and linearizing the system model, the optimal Linear Quadratic Regulator (LQR) controller design process for the linear system was performed and the optimal controller performance was obtained. Finally, to achieve a more favorable control response, considering the limitation of the control signal and applying a change in the weighted matrix Q in the cost function, the speed of the control response increased and overshoot was reduced. This new hybrid topology simplified and cheapened the structure of magnetic levitation (maglev) and reduced the need for control systems and sensors. Furthermore, the electromagnetic coupling effect was resolved in this structure due to the integrated performance of suspension and guidance by one system.

References

1. Lee, H.W., Kim, K.C., and Lee, J. "Review of maglev train technologies", *IEEE Transactions on Magnetics*, **42**(7), pp. 1917–1925 (2006).

2. Wang, L., Yu, P., Li, J., et al. "Suspension system status detection of maglev train based on machine learning using levitation sensors", In *Control And Decision Conference (CCDC)*, 2017 29th Chinese, pp. 7579–7584, IEEE (2017).

3. Lai, Q., Liu, J., Haghani, A., et al. "Energy-efficient speed profile optimization for medium-speed maglev

trains", *Transportation Research Part E: Logistics and Transportation Review*, p. 141, 102007 (2020).

4. Hasirci, U., Balikci, A., Zabar, Z., et al. "3-D FEM analysis of a novel magnetic levitation system", *IEEE Transactions on Plasma Science*, **43**(5), pp. 1261–1265 (2015).

5. Nasiri-Zarandi, R., and Hekmati, A. "A review of suspension and traction technologies in maglev trains", *2019 International Power System Conference (PSC)*, IEEE (2019).

6. Hasirci, U., Balikci, A., Zabar, Z., et al. "Experimental performance investigation of a novel magnetic levitation system", *IEEE Transactions on Plasma Science*, **41**(5), pp. 1174–1181 (2013).

7. hen, Q., Tan, Y., Li, J., et al. "Model-guided data-driven decentralized control for magnetic levitation systems", *IEEE* Access 6, pp. 43546–43562 (2018).

8. Qiang, C., Shao-ke, L., and Jie, L. "Control method research on combined-levitation-and-propulsion system used in maglev vehicles", In *Chinese Automation Congress (CAC)*, IEEE, pp. 487–490 (2013).

9. Kuptsov, V., Fajri, P., Magdaleno-Adame, S., et al. "A new system of combined propulsion and levitation for maglev transportation", *2020 IEEE Applied Power Electronics Conference and Exposition (APEC)*, IEEE (2020).

10. Yoshida, K., Yoshida, T., Manabe, S., et al. "Control of new PM LSM maglev vehicle based on analysis of pitching torque and propulsion force", *2007 IEEE International Symposium on Industrial Electronics*, IEEE (2007).

11. Lu, Y.S. and Berkelman, P. "Design and evaluation of state and disturbance observers for a multivariable magnetic levitation system", *IETE Journal of Research*, **69**(1), pp. 420–437 (2023).

12. Jeong, J.H., Ha, C.W., Lim, J., et al. "Analysis and control of the electromagnetic coupling effect of the levitation and guidance systems for a semi-high-speed maglev using a magnetic equivalent circuit", *IEEE Transactions on Magnetics*, **52**(7), pp. 1–4 (2016).

13. Huang, D., Chen, C., Huang, T., et al. "An active repetitive learning control method for lateral suspension systems of high-speed trains", *IEEE Transactions on Neural Networks and Learning Systems*, **31**(10), pp. 4094–4103 (2019).

14. Tunceroglu, C., Hasirci, U., Maden, D., et al. "The experimental test results of a two-section linear induction launcher", *IEEE Transactions on Plasma Science*, **48**(11), pp. 4041–4047 (2020).

15. Kim, K.B., Levi, E., Zabar, Z., et al. "Restoring force between two noncoaxial circular coils", *IEEE Transactions on Magnetics*, **32**(2), pp. 478–484 (1996).

16. Esfahanian, H.R., Hasanzadeh, S., and Heydari, M. "Performance analysis and force components improvement of an tubular linear induction motor used in a novel magnetic train by 3-D FEM", In *Electrical Engineering (ICEE), Iranian Conference on IEEE*, pp. 1368–1372 (2018).

17. Hasirci, U., Balikci, A., Zabar, Z., et al. "A novel magnetic-levitation system: design, implementation, and nonlinear control", *IEEE Transactions on Plasma Science*, **39**(1), pp. 492–497 (2011).

18. Kwakernaak, H. and Sivan, R., *Linear Optimal Control Systems*, **1**., New York: Wiley-Interscience (1972).

Biographies

Hamid Reza Esfahanian received the BSc degree from K. N. Toosi University of Technology, Tehran, Iran and the MSc degree from Qom University of Technology, Qom, Iran in 2013 and 2017, respectively, both in Electrical Engineering. His research interests include design, modeling, and control of power electronics converters and their application to electrical traction systems.

Saeed Hasanzadeh received the BSc degree from Shahroud University of Technology, Shahroud, Iran in 2003 and the MSc and PhD degrees from University of Tehran, Tehran, Iran in 2006 and 2012, respectively, all in Electrical Engineering. He joined the Faculty of Electrical and Computer Engineering, Qom University of Tehchnology as an Assistant Professor in 2013. His research interests include power electronics, inductive power transfer systems, electrical machines and drives, electric vehicles, and magnetic levitation systems.

Mojtaba Heydari received the undergraduate and graduate degrees from Kashan University, Isfahan; Iran University of Science and Technology, Tehran, Iran; and Tarbiat Modares University, Tehran, all in Electrical Engineering. From 2012 to 2013, he served as a Research Scholar at the Power Electronics Laboratory, University of California at Irvine, Irvine, CA, USA. Since 2014, he has been with the Faculty of Electrical and Computer Engineering, Qom University of Technology, Qom, Iran. His current research interests include power electronics, renewable energy systems, and motor drives.

Josep M. Guerrero received the BSc degree in Telecommunications Engineering, the MSc degree in Electronics Engineering, and the PhD degree in Power Electronics from the Technical University of Catalonia, Barcelona, Spain in 1997, 2000, and 2003, respectively. Since 2011, he has been a Full Professor with the Department of Energy Technology, Aalborg University, Aalborg, Denmark, where he is responsible for the

Microgrid Research Program. His research interests include different microgrid aspects, including power electronics, distributed energy storage systems, hierarchical and cooperative control, energy management systems, smart metering, the Internet of Things for ac/dc microgrid clusters, and islanded minigrids.